J. Phys. B: At. Mol. Opt. Phys. **31** (1998) 3027–3041. Printed in the UK PII: S0953-4075(98)91029-X

Electron-impact excitation of the $\left(\ldots 6s6p\ {}^1P_1\right)$ level in ytterbium

P V Johnson†, Y Li†, P W Zetner†, G Csanak‡, R E H Clark‡ and J Abdallah Jr‡

† Department of Physics, University of Manitoba, Winnipeg, MB, R3T 2N2 Canada

‡ Los Alamos National Laboratory, Los Alamos, NM 87545, USA

Received 26 January 1998

Abstract. We have measured and calculated differential cross sections for electron-impact excitation of the $\left(\ldots 6s6p\ {}^1P_1\right)$ level in ytterbium at collision energies of 5, 10, 20, 40 and 80 eV. Calculations were made in the unitarized distorted-wave approximation. Measurements of the relative differential cross section, taking account of volume correction effects, were placed on an absolute scale by normalization to the theoretical integral cross section at 80 eV with extrapolation to lower energies based on the measured excitation function of Shimon *et al* (1981 *Opt. Spektrosk.* **50** 571). Excellent agreement between theory and experiment is obtained in the regime of low momentum transfer.

1. Introduction

Relatively little is known about electron scattering from the lanthanide atoms. Ytterbium is an interesting member of this group for a variety of reasons. This atom has a closed-shell, two (6s) valence electron, ground level configuration: $\left(1s^2 2s^2 2p^6 3s^2 3p^6 3d^{10} 4s^2 4p^6 4d^{10} 5s^2 5p^6 4f^{14} 6s^2\right)^1S_0$, and many electron energy-loss spectral features are, therefore, relatively straightforward to identify. In this paper atomic levels are identified by the designations of Martin *et al* (1978) which give the dominant valence electron configuration and a ${}^{2S+1}L_J$ term.

Calculational approaches applied with some success to the treatment of intermediate energy electron scattering from closed-shell atoms, such as the first-order perturbation theories described by Srivastava *et al* (1992, 1994), Clark *et al* (1989) and Bartschat and Madison (1987), should be suitable for this atom as well. Furthermore, ytterbium is a heavy atom ($Z = 70$) and can therefore provide a testing ground for the importance of relativistic effects in electron–atom scattering. Relativistic effects (i.e. spin–orbit coupling) are certainly important in the description of the atomic wavefunctions since the ($J = 1$) P states appear to be well characterized by the 'intermediate' coupling scheme. We also point out that the (nominal) $\left(\ldots 6s6p\ {}^3P_1\right)$ level in this atom can be prepared by dye laser excitation to allow the investigation of electron scattering from this excited state. The feasibility of superelastic scattering measurements from the laser-prepared $\left(\ldots 6s6p\ {}^3P_1\right)$ state has recently been demonstrated (Li and Zetner 1994). From a practical standpoint studies of electron impact on ytterbium are important because of the potential suitability of ytterbium vapour as a laser medium (Klimkin 1975).

The only electron scattering cross section data available for this element come from the work of Shimon *et al* (1981) who have produced optical excitation functions for

 © 1998 IOP Publishing Ltd

important atomic transitions. Relative differential cross sections have been measured by Kazakov and Khristoforov (1981) for near-threshold impact energies and scattering angle $\theta = 90^\circ$. The aim of the work was to investigate strong resonance features in the $\theta = 90^\circ$ excitation functions for elastic scattering and for the excitation of the $\left(\ldots 6s6p\ {}^1P_1\right)$ and $\left(\ldots 6s6p\ {}^3P_{0,1,2}\right)$ levels. More recently, Mandy *et al* (1993) have presented energy-loss spectra and a threshold excitation spectrum obtained using a hypocycloidal electron spectrometer, while Li and Zetner (1994) have measured electron-impact coherence parameters (EICP) for the $\left(\ldots 6s6p\ {}^3P_1\right)$ excitation. Previous theoretical studies are limited to the recent work of Srivastava *et al* (1995) who calculated intermediate energy differential cross sections (DCS), EICP and various spin parameters for the excitation of $(J = 1)$ P states in the relativistic distorted-wave (RDW) approximation.

In the present investigation we have measured the DCS for excitation of the $\left(\ldots 6s6p\ {}^1P_1\right)$ level using conventional crossed-beam methods. Supporting atomic structure calculations have been carried out to aid in the identification of observed features in the energy loss spectra. Scattering calculations making use of the unitarized distorted-wave approximation (UDWA) were also undertaken for comparison with the measured results. Details of the experimental procedure and the method of calculation are presented below.

2. Details of the calculational method

The present calculations are similar to those described by Clark *et al* (1989) in their investigation of the Ba atom. Some of the essential points are summarized here.

The atomic structure calculation (by the CATS code) is based on the method developed by Cowan (1968a, b, 1981) and Cowan and Griffin (1967). Radial wavefunctions for a single configuration are calculated by a Hartree–Fock scheme in which the configuration average energy is minimized. This calculation is essentially non-relativistic except for the inclusion of the mass and Darwin terms. Mixing among all configurations and LS terms with the same parity and the same total electronic angular momentum J is obtained through perturbation theory. The present structure calculation made use of 22 configurations. These involved a $\left(1s^2 2s^2 2p^6 3s^2 3p^6 3d^{10} 4s^2 4p^6 4d^{10} 5s^2 5p^6 4f^{14}\right)$ core with valence electrons in the two-electron configurations: $6s^2$, $6p^2$, $5d^2$, 5d7s, 6s5d, 6s6d, 6s7d, 5d6d, 5d7d, 6p7p, 6s7s,

Table 1. Calculated energy levels for excitation energies below ~ 4 eV.

	Energy (eV)	
Level	CATS (this work)	Martin *et al* (1978)
$6s6p\ {}^3P_0$	1.867	2.144
$6s6p\ {}^3P_1$	1.922	2.231
$6s6p\ {}^3P_2$	2.051	2.444
$6s6p\ {}^1P_1$	2.992	3.108
$6s5d\ {}^3D_1$	2.997	3.036
$6s5d\ {}^3D_2$	3.029	3.069
$6s5d\ {}^3D_3$	3.097	3.133
$6s5d\ {}^1D_2$	3.299	3.432
$6s7s\ {}^3S_1$	3.910	4.054
$6s7s\ {}^1S_0$	4.111	4.259

6s8s, 6s6p, 6s7p, 6s8p, 6s9p, 6p5d, 6p6d, 6p7s, 6p8s, 6p7d and 6p8d. Wavefunctions and level energies for 153 levels were calculated. Table 1 gives a gives a list of calculated energy levels (including dominant configuration, dominant LS terms and level energy) for excitation energies below approximately 4 eV. For comparison, the spectroscopically determined level energies of Martin *et al* (1978) are also given. The dominant contributing configurations and LS terms of the relevant levels are:

(i) for the $(\ldots 6s^2\ ^1S_0)$ level:

$$0.9766(\ldots 6s^2\ ^1S_0) + 0.1875(\ldots 6p^2\ ^1S_0) - 0.0682(\ldots 5d^2\ ^1S_0) - 0.0508(\ldots 6s7s\ ^1S_0) + 0.0482(\ldots 6p7p\ ^1S_0) - 0.0279(\ldots 5d6d\ ^1S_0) - 0.0232(\ldots 6s8s\ ^1S_0) - 0.0162(\ldots 5d7d\ ^1S_0)$$

and

(ii) for the $(\ldots 6s6p\ ^1P_1)$ level:

$$0.9358(\ldots 6s6p\ ^1P_1) - 0.3112(\ldots 5d6p\ ^1P_1) - 0.1261(\ldots 6s7p\ ^1P_1) + 0.0758(\ldots 6s6p\ ^3P_1) - 0.0552(\ldots 6s8p\ ^1P_1) - 0.0341(\ldots 6s9p\ ^1P_1) + 0.0285(\ldots 6p7s\ ^1P_1) - 0.0112(\ldots 5d6p\ ^3D_1).$$

Additionally, the oscillator strength of the $(\ldots 6s6p\ ^1P_1)$ to $(\ldots 6s^2\ ^1S_0)$ radiative transition was calculated to be 2.424. (Oscillator strengths were calculated in the length form only.)

Electron collision calculations were performed using the atomic structure data. We employed the distorted-wave approximation of Mann (1983) in which the continuum wavefunction for the incident (scattered) electron is calculated in the potential of the initial (final) configuration. Reactance matrix elements were first calculated between LS terms and unitarization of the reactance matrix was then carried out (Saraph *et al* 1969, Davis *et al* 1976, Mann 1983, equation (4)) to give the unitarized distorted-wave approximation (UDWA). Recoupling of the matrix elements was performed using the pair-coupling scheme (Saraph 1972, Clark 1978, Mann 1983) with the inclusion of configuration-interaction and intermediate-coupling mixing. For the present differential cross sections the wavefunction of the continuum electron was expanded in 300 partial waves.

3. Experimental procedure

Figure 1 gives a schematic diagram of our experimental arrangement. The electron spectrometer consists of an electron source and scattered electron detector both employing standard, single-hemispherical energy selection optics. Overall system energy resolution of about 80 meV (FWHM) was maintained for these measurements. The electron beam current was approximately 150 nA. The scattering apparatus is housed in a single layer (1.27 mm) mu-metal shield to give uniform, residual magnetic fields of less than 25 mG in all directions near the interaction volume.

The metal vapour beam source consists of a tubular stainless steel crucible wrapped with resistive coaxial heating wire to give a stable operating temperature of about 600 °C. The crucible resides in a stainless steel thermal shield with an aperture to pass the metal vapour beam. Collimation of the beam is determined by an orifice in the crucible of 12.7 mm in length and 0.8 mm in diameter, and a 0.8 mm diameter aperture on the thermal shield which is located 12.7 mm away from the interaction region. The metal vapour beam width

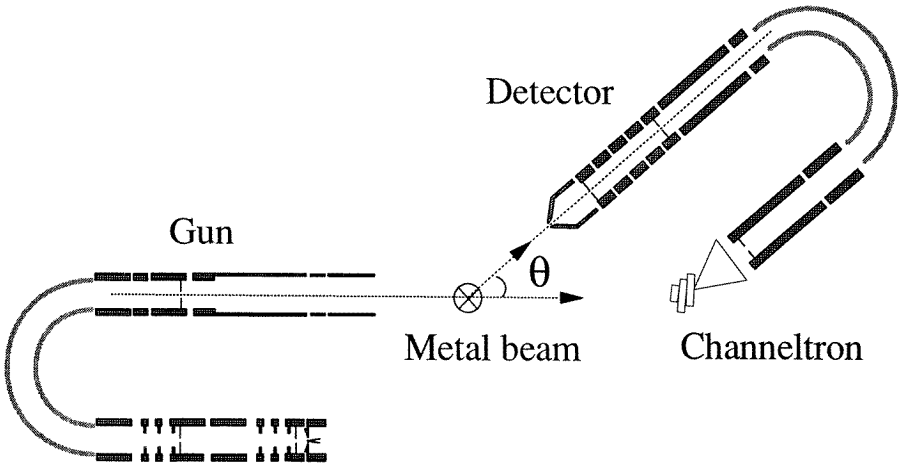

Figure 1. A schematic diagram of the electron scattering apparatus. Arrows show the direction of incident and scattered electrons with the scattering angle, θ, indicated. The metal vapour beam is directed into the plane of the figure.

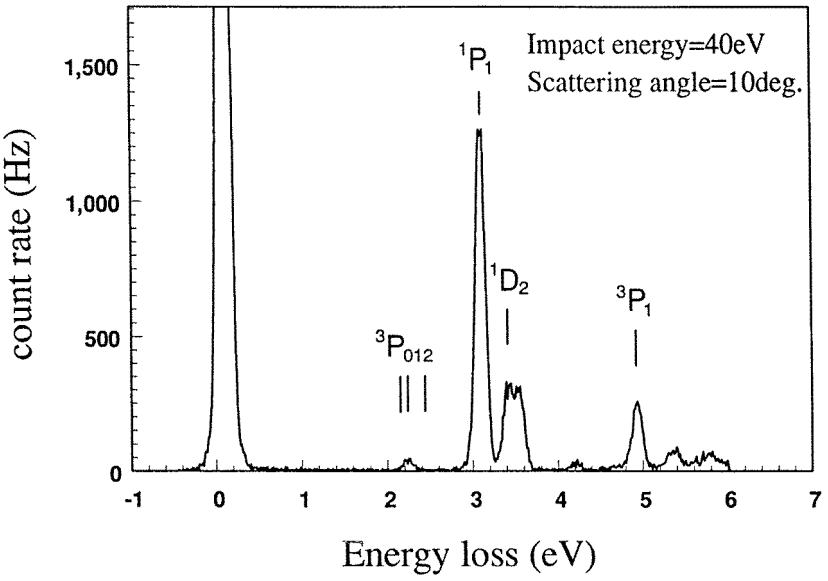

Figure 2. A typical electron energy-loss spectrum obtained with the electron scattering apparatus.

at the interaction region was measured to be approximately 1.6 mm (FWHM) by means of projecting the beam onto a clean metal surface and analysing the (circular) pattern of deposited Yb. At operating temperature, the typical target density was estimated to be 2×10^{13} cm^{-3}. The metal vapour beam was directed perpendicularly to the scattering plane to minimize any angular dependence on the size of the interaction volume (as discussed below).

Before actual DCS measurements, calibration of the impact energy and calibration of the zero scattering angle were done. The impact energy was calibrated against the known excitation energy of the helium $2\,^2S$ elastic scattering resonance (19.37 eV) at scattering angle $\theta = 90^\circ$. The zero scattering angle was found by maximizing the inelastic scattering count rate of the $(\ldots 6s6p\ ^1P_1)$ feature. The 0° scattering angle determined in this way differed by 3° from its value determined by optical alignment of the gun and detector.

For our differential cross section measurements, the scattering intensity associated with the electron collisional excitation of the $(\ldots 6s6p\ ^1P_1)$ level was measured as a function of the scattering angle at fixed impact energies. The measurements were performed at incident electron kinetic energies (impact energies) $E_0 = 5, 10, 20, 40$ and 80 eV and at various scattering angles ranging from 2° to 70°. At each scattering angle and impact energy, an energy-loss spectrum was accumulated. Furthermore, the ratemeter reading of $(\ldots 6s6p\ ^1P_1)$ inelastic electron scattering signal at 10° was taken as a reference to minimize the influence of instrumental drift during the measurement. The relative differential cross section was obtained by integrating the $^1P_1$ energy-loss feature profile and normalizing the integration to the count rate at the 10° reference angle. At any given scattering angle, frequent cross-checks of this type were made. An energy-loss spectrum at impact energy of 40 eV and scattering angle of 10° is shown in figure 2.

4. Data analysis

Our raw measurements consist of angular distributions of inelastic scattering intensity, i.e. a relative DCS. Before normalizing the relative DCS to an absolute scale, we carried out numerical modelling calculations to account for the effect of scattering geometry dependence on the scattering angle. In a crossed-beam experiment of the type carried out here, the measured signal arises from a spatial region (the 'interaction region' or 'interaction volume') defined by the overlap of the electron beam, the target atomic beam and the detection viewcone. This overlap can change with scattering angle and, as a result, distort the measurement of the relative DCS. The goal of our modelling calculation was to calculate an appropriate correction factor which could be applied to the measured relative DCS. Considerations of this type have been explored in detail by Brinkmann and Trajmar (1981).

In the present approach, we utilized a numerical scheme in which the target volume is modelled by a three-dimensional lattice of points representing an array of discrete scatterers. The contribution to detected scattering signal from any one of these points is determined by a weighting coefficient which reflects the spatial distributions of electron beam current and atom beam density. We assumed parallel beams with Gaussian spatial profiles whose widths we determined by measurement. In the case of the electron beam we employed the scattered electron detector as a Faraday cup and measured the angular dependence of the transmitted current at the various impact energies. The atom beam profile was determined as explained above.

Our modelling calculation also accounted for the fact that the detection of scattered electrons originating at a particular lattice point can occur for a range of possible scattering angles, limited by the extent of the detection viewcone. In our model, a scattered electron trajectory corresponding to a specific scattering angle was weighted according to an angular distribution of detection efficiency through the detection viewcone as well as the calculated DCS value associated with this particular scattering angle. The detection viewcone is limited to 6.3° by two collimating apertures and we chose a Gaussian distribution of 6° FWHM to represent a weak variation in detection efficiency across the viewcone.

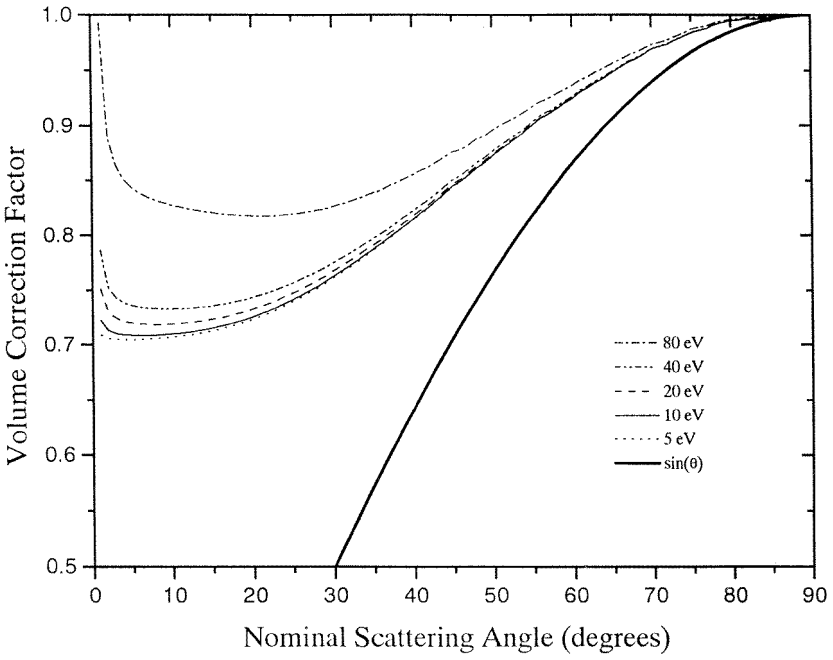

Figure 3. Volume correction factors obtained by the numerical method described in the text. These were applied to the relative DCS measurements at the indicated impact energies.

The correction factors obtained with this modelling approach and applied to the measurements are plotted in figure 3 for various impact energies (the impact energy dependence arises through the utilization of the appropriate UDWA DCS) and are compared with the $\sin\theta$ correction applied to measurements using a gas cell target. The calculated correction factors are quite similar in behaviour to those given by Brinkmann and Trajmar (1981).

To place the measured, volume-corrected, relative DCS on an absolute scale, we attempted a normalization to the integral cross sections (ICS) measured by Shimon *et al* (1981). Their measurement of optical excitation functions was conducted using the method of intersecting atomic and electron beams and the photoelectric detection of the spectral line intensities. The excitation functions for spectral lines of the strongest transitions were given in their work. We found that their cross sections for the 3988 Å transition at impact energies ranging from 5 to 80 eV are approximately one order of magnitude smaller than the present UDWA ICS results (as shown in table 2). Even larger discrepancies with the RDW theory of Srivastava *et al* (1995) are apparent in table 2. Based on the success of the UDWA scheme in predicting the DCS and ICS for the $\mathrm{Ba}(\ldots 6s6p\ ^1P_1)$ excitation at higher impact energies (20–100 eV) (Clark *et al* 1989) we chose to explore alternate normalization schemes.

The generalized oscillator strength (GOS) method has been used for the normalization of relative DCS measurements. The basis of this method is the work done by Lassettre *et al* (1969) in which it is shown that the GOS converges to the optical oscillator strength (OOS) in the limit of zero momentum transfer, i.e. $K^2 \rightarrow 0$. This then presents the possibility of converting relative DCS measurements into relative GOSs and using the appropriate

Table 2. Yb integral cross sections ($\times 10^{-16}$ cm^2).

E_0	Line excitation cross sections							
(eV)	3988 Å	6668 Å	4394 Å	4932 Å	$(\ldots 6s6p\ ^1P_1)^a$	$(\ldots 6s6p\ ^1P_1)^b$	$(\ldots 6s6p\ ^1P_1)^c$	$(\ldots 6s6p\ ^1P_1)^d$
80	2.14	0.076	0.032	0.0054	2.03	20.4	21.9	20.4
40	3.29	0.14	0.068	0.0068	3.08	32.1	40.0	31.0
20	4.62	0.22	0.14	0.0083	4.25	41.1	58.5	42.7
10	4.36	0.26	0.12	0.0046	3.98	38.7	62.5	40.0
5	0.84	—	—	—	0.84	31.9	88.1	8.4

[a] Shimon *et al* (1981) (cascade corrected).
[b] UDWA (this work).
[c] RDW (Srivastava *et al* 1995).
[d] Shimon *et al* (1981) (renormalized).

OOS to normalize the data into absolute terms. The first problem arises from the fact that the minimum value of K^2 is determined by the level excitation energy and, hence, the $K^2 \rightarrow 0$ limit is an unphysical one. This is complicated by the discovery that, at low impact energies, measured GOS values increase rapidly as $K^2 \rightarrow 0$, making extrapolation into the unphysical region a matter of guess work. In an attempt to circumvent this problem Msezane and Sakmar (1994) have derived rigorous bounds on K^2 and used them to construct a universal formula that would extrapolate the GOS through the unphysical region to the OOS regardless of impact energy. Unfortunately, when we attempted to use the method we could not achieve a satisfactory fit of our data to the universal curve and decided to abandon this approach. We note that the efficacy of the GOS extrapolation method of Msezane and Sakmar has recently been challenged by Williams and Stelbovics (1997). See also the rebuttal comment by Msezane and Bessis (1997).

The normalization procedure which we finally adopted hinges on the value of the UDWA ICS calculated at 80 eV. Our confidence in this theoretical value as a normalization point derives from (i) previous success in calculating the Ba$(\ldots 6s6p\ ^1P_1)$ DCS and ICS at higher impact energies (Clark *et al* 1989) and (ii) the observation that ICS values calculated in the UDWA and RDW frameworks begin to converge with increasing impact energy.

The first step of our normalization procedure involved the use of the UDWA ICS at 80 eV impact energy to renormalize the 'cascade-corrected', optical excitation function measured by Shimon *et al* (1981). Allowance for the cascade component of their measured excitation function was made by subtracting contributions from the $(\ldots 6s6d\ ^1D_2)$ level and $J = 2$ levels at excitation energies 47 822 and 45 338 cm^{-1} (5.93 and 5.62 eV, respectively) which radiatively decay to the $(\ldots 6s6p\ ^1P_1)$ level and whose optical excitation functions (at wavelengths 6688, 4394 and 4932 Å, respectively) were also measured by Shimon *et al* (1981) (features number 6, 28 and 30 in their table 1). The renormalized ICS values (given in table 2) were then used as the calibration standards for our DCS measurements at impact energies of 5, 10, 20 and 40 eV. In other words, we assume that the shape but not the magnitude of the measured excitation function is correct.

5. Results and discussion

Our experimental and theoretical (UDWA) determinations of the Yb$(\ldots 6s6p\ ^1P_1)$ DCS are presented in figures 5–9. The RDW calculations of Srivastava *et al* (1995) are also

Table 3. DCS measurements (with uncertainties) for scattering angles from 2° to 65°.

Scattering angle (deg)	DCS ($\times 10^{-16}$ cm^2 sr^{-1})				
	5 eV	10 eV	20 eV	40 eV	80 eV
2	13.3(2.7)	—	835(166)	1016(199)	1175(236)
3	—	205(40)	—	774(150)	583(116)
4	—	—	572(109)	539(103)	325(63)
5	12.9(2.6)	191(36)	453(87)	342(65)	191(41)
6	—	—	354(66)	231(43)	99.4(22)
7	12.3(2.6)	174(32)	—	154(28)	56.5(12)
8	—	—	197(36)	99.6(18)	31.8(7.0)
9	—	—	—	65.2(12)	—
10	10.8(2.4)	135(24)	108(19)	42.1(7.5)	9.62(2.6)
12	—	—	—	—	3.30(0.83)
15	6.63(1.3)	54.2(9.2)	21.3(4.2)	5.77(0.96)	1.51(0.32)
20	4.06(0.74)	18.4(2.9)	5.79(0.96)	1.28(0.20)	0.74(0.15)
25	2.29(0.38)	6.93(1.0)	1.63(0.27)	0.72(0.10)	0.31(0.086)
30	1.23(0.17)	2.87(0.39)	0.65(0.13)	0.47(0.064)	0.12(0.065)
35	—	1.32(0.19)	0.39(0.076)	0.24(0.029)	0.063(0.044)
40	0.52(0.063)	0.83(0.10)	0.27(0.049)	0.14(0.016)	0.041(0.028)
45	—	—	0.20(0.045)	0.088(0.009)	0.027(0.019
50	0.37(0.037)	0.48(0.088)	0.15(0.053)	0.059(0.005)	—
52	—	—	—	0.050(0.004)	—
55	—	—	0.11(0.062)	0.040(0.003)	—
60	0.38(0.031)	—	0.091(0.071)	0.028(0.002)	—
65	0.34(0.043)	0.26(0.073)	0.008(0.007)	—	—

shown. Error bars shown on our experimental values reflect the uncertainty associated with measurement of the *relative* DCS. This arises from: (i) counting statistics and (ii) the application of our calculated volume correction to the relative DCS measurement. Uncertainty in the volume correction arises through the sensitivity of the numerical modelling procedure to experimental parameters, some of which can be measured (e.g. electron beam and atom beam spatial distributions) and some of which must be estimated (transmission efficiency through the detection viewcone). Analysis of the modelling results for their dependence on reasonable variations in the model parameters led us to assume a 20% error contribution at the lowest scattering angle studied (2°) which decreases (linearly) to zero at 90° scattering angle. Table 3 summarizes the measured DCS data with uncertainties given by the error in the relative DCS measurements (same as the error bars in figures 5–9).

Absolute values of the DCS are determined by normalization to the UDWA ICS at 80 eV impact energy and we ascribe no error to this theoretical calibration point. Uncertainty in the normalization procedure then arises essentially from the following sources: (i) the extrapolation approximations used to extend our measured DCS values to 0° and 180° scattering angle for the purpose of integration and (ii) measurement uncertainty in the relative excitation function published by Shimon *et al* (1981) (including uncertainty in our estimates of the cascade contributions).

Three distinct angular regions were involved in converting the relative DCS measurements to ICS values. Measured data points covered the angular ranges: 2° → 50° at 80 eV, 2° → 60° at 40 eV, 2° → 65° at 20 eV, 3° → 65° at 10 eV and 2° → 65° at 5 eV. Measured data in these regions were integrated by fitting a cubic spline curve to the data points and integrating the curve. To integrate the forward scattering region (i.e. the

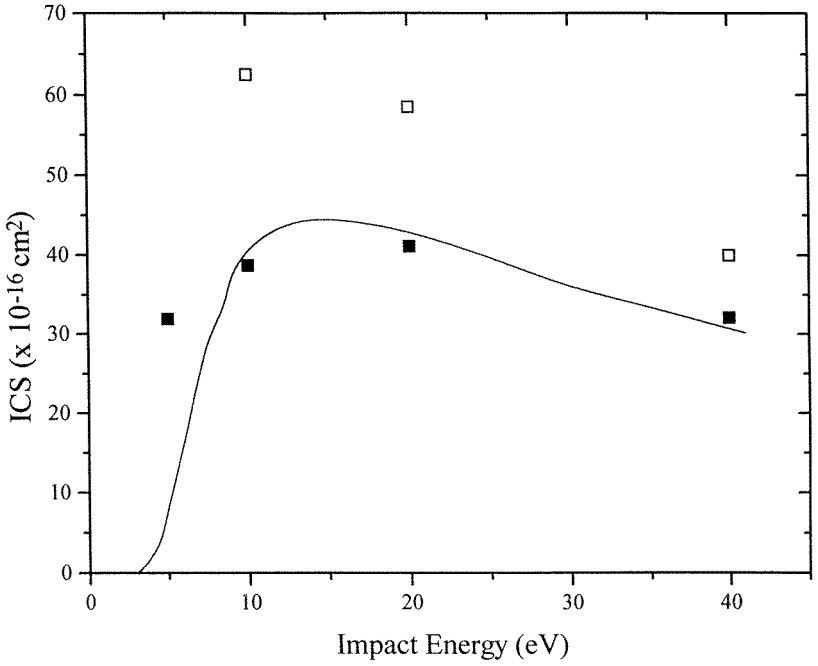

Figure 4. Integral cross sections (ICS) for excitation of the Yb$(\ldots 6s6p\ ^1P_1)$ level: ——, measured ICS of Shimon *et al* (1981) corrected for cascade and renormalized to UDWA theory at 80 eV as discussed in the text; ■, results of the UDWA calculation; □, RDW results of Srivastava *et al* (1995).

region from 0° to the lowest angle measured) the shape (i.e. angular dependence) of the UDWA DCS was used for extrapolation. To extend the integral to high angles (namely, from the highest angle measured to 180°) the DCS for impact energies 5, 10, 20 and 40 eV was assumed to take on a constant value equal to the value found at the highest measured angle.

Although the extrapolation approximation used to treat high angles is very crude, the maximum contribution of the integral over this region to the overall ICS was calculated to be 2.5% at 40 eV, 3.1% at 20 eV, 6.9% at 10 eV and 40% at 5 eV. This maximum contribution was determined by choosing the constant, extrapolated, value to be given by the upper error limit of the relative DCS measured at the largest scattering angle. The highly forward-peaked nature of the DCS at the higher impact energies (10, 20 and 40 eV) significantly diminishes the contribution from high-angle scattering and legitimizes, to some extent, the crude extrapolation employed at these energies. Note, however, that the 5 eV case presents serious problems.

In the case of our 80 eV data, a different extrapolation into the high-angle region was employed. The excellent agreement in angular behaviour between our 80 eV relative DCS measurements and the UDWA results prompted us to make use of the DCS shape predicted by UDWA theory in the high-angle region. Integration over the high-angle region for this impact energy contributes 0.8% to the ICS. As a measure of the error involved in integrating our measured relative DCS, we chose to take the value of maximum percentage contributions of the integrals over the high-angle extrapolated regions, as listed above.

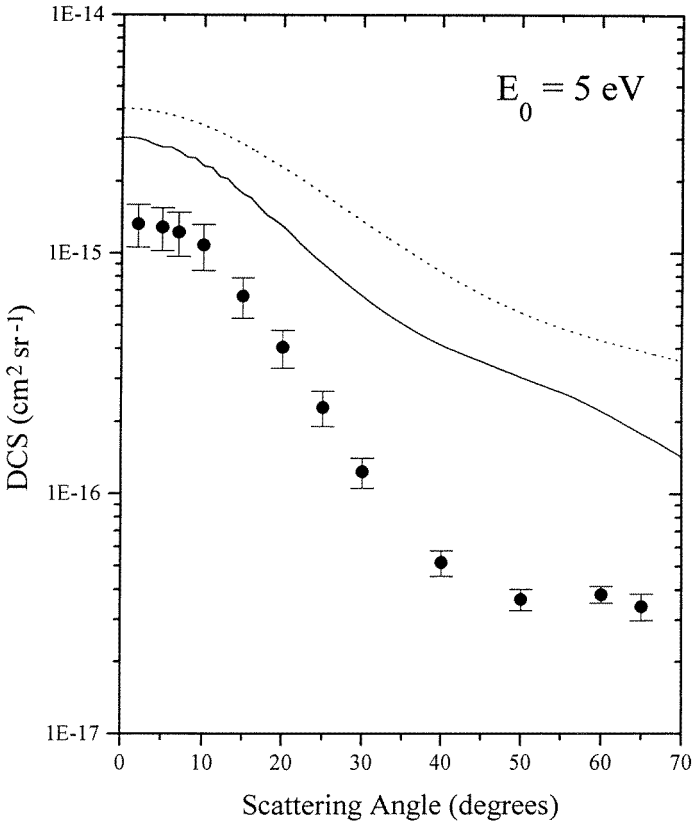

Figure 5. Differential cross sections for excitation of the Yb$(\ldots 6s6p\ ^1P_1)$ level at an impact energy of $E_0 = 5$ eV. The experimental data are represented by the full circles with error bars: ——, UDWA results; – – –, RDW results of Srivastava *et al* (1995).

Further sources of uncertainty in the normalization of our relative DCS arise from the error in the relative excitation function of Shimon *et al* (1981) and uncertainty in our estimation of the cascade component affecting their measurement. Shimon *et al* (1981) quote an error of 5% in their measured relative excitation function. Additionally, they have measured optical excitation functions for three spectral lines arising from levels which feed the $(\ldots 6s6p\ ^1P_1)$ level by radiative cascade. They quote an uncertainty of 30% in these measurements. We have estimated the cascade component from these three contributing levels to be 5% at 80 eV, 6% at 40 eV, 8% at 20 eV, 9% at 10 eV and negligible at 5 eV. Given the possibility of further, unmeasured, cascade contributions, we ascribe an uncertainty of 50% to the above values (in addition to the 30% estimated error of the line excitation cross sections). This leads to uncertainties in the calibration ICS values of 3% at 80 eV, 4% at 40 eV, 5% at 20 eV and 6% at 10 eV based on cascade considerations alone. Addition, in quadrature, of all errors associated with the normalization of our relative experimental DCS gives: 6% at 80 eV, 7% at 40 eV, 8% at 20 eV, 11% at 10 eV and 40% at 5 eV. As mentioned above, these error estimates rely on the assumption of no uncertainty in the ICS obtained by the UDWA method at 80 eV.

Having discussed our error analysis in detail we can proceed to describe some general features of our results. Examination of table 2 and figure 4, for example, shows that

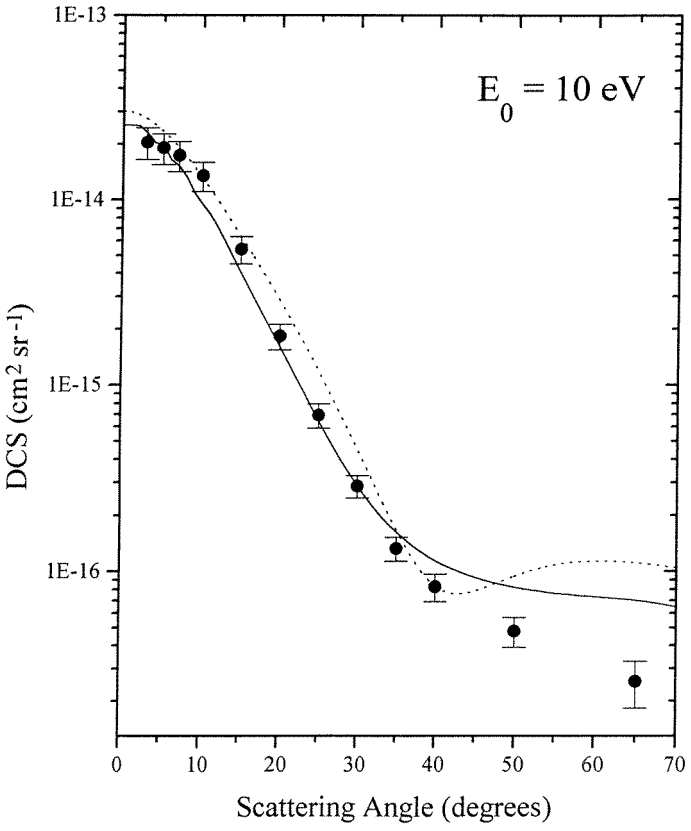

Figure 6. Same as figure 5, except $E_0 = 10$ eV.

integral cross sections computed within the UDWA framework agree closely with Shimon *et al*'s (1981) results at impact energies of 10, 20 and 40 eV once cascade correction and renormalization to the UDWA ICS at 80 eV have been carried out. In other words, the energy dependence of the integral cross section as measured by Shimon *et al* (1981) is reproduced by UDWA theory over the 10–80 eV range of impact energies. This agreement also tends to support our treatment of the cascade contribution at these energies. Note, however, the glaring discrepancy between the experimentally observed and calculated ICS at 5 eV impact energy. This is discussed further below.

Turning our attention to figures 5–9 we can make the following general statements. We note that the agreement between the measured DCS and that obtained by the UDWA calculation is excellent for smaller scattering angles (less than about 25°) at impact energies of 20 eV and higher. Furthermore, the discrepancy between theory and experiment at larger scattering angles is dramatically improved as impact energy increases. In particular, the agreement in angular behaviour at 80 eV impact energy is excellent over all measured angles: $2^\circ \rightarrow 50^\circ$. Comparison of DCS magnitudes is not too meaningful here because the ICS determined by the UDWA scheme served as the calibration point at this energy. These observations are consistent with the expected regime of validity of first-order, perturbative theories like the UDWA, namely the low momentum-transfer regime.

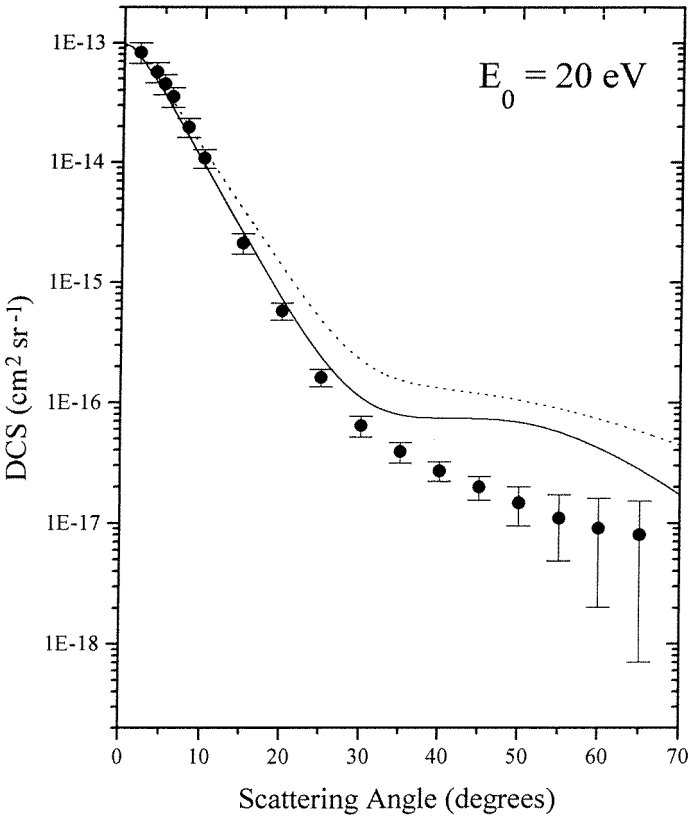

Figure 7. Same as figure 5, except $E_0 = 20$ eV.

At 10 eV impact energy we note, despite the agreement between the UDWA and renormalized Shimon *et al* (1981) ICS, the measured DCS is not well reproduced by the UDWA calculation for near-forward scattering angles. Agreement between the UDWA and measured DCS is excellent, however, in the range of scattering angles $15^\circ < \theta < 30^\circ$. The situation becomes far less satisfactory at 5 eV impact energy. Here, problems are already apparent in a factor of 4 discrepancy between the UDWA and renormalized Shimon *et al* (1981) ICS values. Part of the problem may arise from the fact that the integral cross section is rapidly varying with energy in this near-threshold region and the experimentally determined ICS will be sensitive to the impact energy calibration. A rough check on the impact energy scale of Shimon *et al* (1981) was performed by fitting a linear energy dependence to their measured excitation function in the near-threshold region (4.8–7.5 eV) and extrapolating to threshold. The extrapolated value of the excitation threshold was found to be 4.1 eV in contrast to the spectroscopically determined value of 3.11 eV. If the suggested correction of 1.0 eV is applied to the energy scale of Shimon *et al* (1981), then the 5 eV cross section more than doubles in value (to 1.7×10^{-16} cm^2), thereby alleviating somewhat the discrepancy between theory and experiment. The effect of such a scale correction on the ICS measured at higher energies is negligible (5% at 10 eV, and $< 3\%$ at 20, 40 and 80 eV).

Comparison of the 5 eV UDWA results with the DCS in figure 3 reveals a large discrepancy in magnitude which reflects the disagreement with the ICS value used for

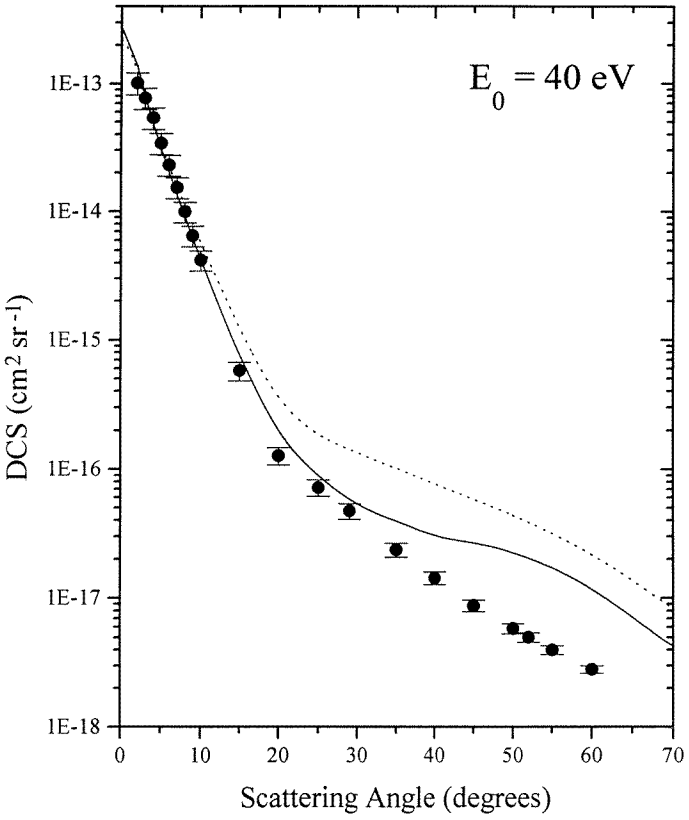

Figure 8. Same as figure 5, except $E_0 = 40$ eV.

calibration. An additional source of error may arise from the rather crude approximation used to extrapolate the experimental DCS to high angles. In the case of our 5 eV data, the extrapolated high-angle region accounts for 40% of the integrated cross section. We do note, however, that the angular behaviour of the measured 5 eV DCS is well described by the UDWA calculation for near-forward scattering ($<10^\circ$).

It is also important to point out that at 5 eV impact energy (less than 2 eV above the $6\,{}^1P_1$ excitation threshold at 3.11 eV) we are no longer in a regime of low momentum transfer and first-order perturbative theory is of questionable value. At this low impact energy, channel-coupling effects may become important in the excitation and the UDWA approach does not treat these effects adequately.

In comparing the RDW calculations of Srivastava *et al* (1995) to our present work, we note that the RDW theory tends to overestimate both the integral and differential cross sections. The present results and the RDW results converge (faster at smaller scattering angles in the case of the DCS) with increasing impact energy, however, at 80 eV, the UDWA approach still gives a more accurate calculation of the DCS angular behaviour. This suggests that the description of the $\left(\ldots 6s6p\ {}^1P_1\right)$ excitation process may be adequately described in a non-relativistic framework since the collision is treated non-relativistically in the UDWA scheme. Differences between the RDW and UDWA approaches might then be attributable to differences in the atomic wavefunctions employed. Srivastava *et al* (1995) use a $6s^2$

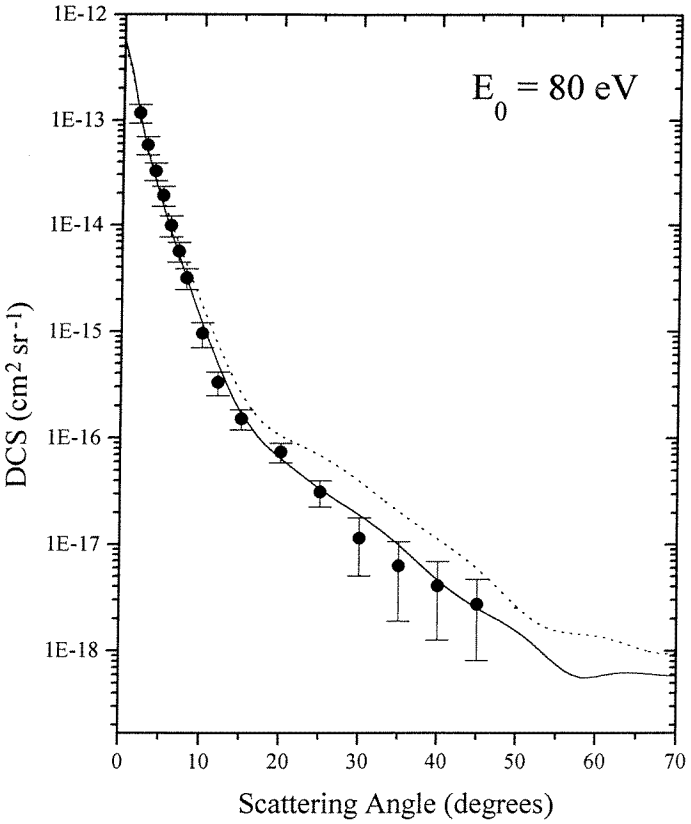

Figure 9. Same as figure 5, except $E_0 = 80$ eV.

valence electron configuration for the ground state and describe the excited ($J = 1$) P states in terms of jj coupling with 6s6p ($j = \frac{1}{2}$) and 6s6p ($j = \frac{3}{2}$) configurations.

6. Conclusions

We have measured and calculated (within the UDWA framework) differential cross sections for electron-impact excitation of the $\left(\ldots 6s6p\ {}^1P_1\right)$ level in ytterbium at impact energies of 5, 10, 20, 40 and 80 eV. Measurements were placed on an absolute scale by calibration with the excitation function of Shimon *et al* (1981) renormalized to the UDWA ICS at 80 eV impact energy. Agreement between experiment and UDWA theory is quite good except at 5 eV.

Acknowledgments

Financial support by the Natural Sciences and Engineering Council of Canada is gratefully acknowledged by PWZ. PVJ and YL acknowledge financial assistance from the Graduate Fellowship program of the University of Manitoba. GC, REHC and JA acknowledge the financial support of the US Department of Energy.

References

Bartschat K and Madison D H 1987 *J. Phys. B: At. Mol. Phys.* **20** 5839
Brinkham R T and Trajmar S 1981 *J. Phys. E: Sci. Instrum.* **14** 245
Clark R E H 1978 *Comput. Phys. Commun.* **16** 119
Clark R E H, Abdallah J Jr, Csanak G and Kramer S P 1989 *Phys. Rev.* A **40** 2935
Cowan R D 1968a *J. Opt. Soc. Am.* **58** 808
——1968b *J. Opt. Soc. Am.* **58** 924
——1981 *Theory of Atomic Spectra* (Berkeley, CA: University of California Press)
Cowan R D and Griffin D C 1967 *J. Opt. Soc. Am.* **66** 1010
Davis J, Kepple P C and Blaha M 1976 *J. Quant. Spectrosc. Radiat. Transfer* **16** 1043
Kazakov S M and Khristoforov O V 1983 *Opt. Spektrosk.* **54** 443
Klimkin V G 1975 *Sov. J. Quantum Electron.* **5** 326
Lassettre E N, Skerbele A and Dillon M A 1969 *J. Chem. Phys.* **50** 1829
Li Y and Zetner P W 1994 *J. Phys. B: At. Mol. Opt. Phys.* **27** L293
Mandy J A, Romanyuk M I, Papp F F and Shpenik O B 1993 *Proc. 18th Int. Conf. on the Physics of Electronic and Atomic Collisions (Aarhus)* ed T Andersen, B Fastrup, F Folkmann and H Knudsen (Bristol: Hilger) Abstracts p 167
Mann J B 1983 *At. Data Nucl. Data Tables* **29** 407
Martin W C, Zalubas R and Hagan L 1978 *Nat. Stand. Ref. Data Series: NSRDS-NBS 60* (Washington, DC: US Govt Printing Office)
Msezane A Z and Bessis D 1997 *J. Phys. B: At. Mol. Opt. Phys.* **30** 445
Msezane A Z and Sakmar I A 1994 *Phys. Rev.* A **49** 2405
Saraph H 1972 *Comput. Phys. Commun.* **3** 256
Saraph H, Seaton M J and Shemming J 1969 *Phil. Trans. R. Soc.* **264** 77
Shimon L L, Golovchak N V, Garga I I and Kurta I V 1981 *Opt. Spektrosk.* **50** 571
Srivastava R, McEachran R P and Stauffer A D 1995 *J. Phys. B: At. Mol. Opt. Phys.* **28** 885 and Private communication
Srivastava R, Zuo T, McEachran R P and Stuaffer A D 1992 *J. Phys. B: At. Mol. Opt. Phys.* **25** 3709
Williams J F and Stelbovics A T 1997 *J. Phys. B: At. Mol. Opt. Phys.* **30** 43